Theoretical analysis of Microring-resonator-based biosensor with high resolution and free of temperature influence

Aoqun Jian[1, 2], Haiquan Tang[1, 2], Qianqian Duan[1, 2], Jianlong Ji[1, 2], Qiang Zhang[1, 2], Xuming Zhang[1, 2,*], Shengbo Sang[1, 2, *]

[1] MicroNano System Research Center, Taiyuan University of Technology, Taiyuan 030600, China;
[2] Key Laboratory of Advanced Transducers and Intelligent Control System, Shanxi Province and Ministry of Education, Taiyuan 030600, China
* Correspondence: sangshengbo@tyut.edu.cn; xuming.zhang@polyu.edu.hk

Abstract: The issue of thermal effects is inevitable for the ultra-high refractive index measurement. In this paper, a biosensor with parallel-coupled dual-microring resonator configuration is proposed to achieve high resolution and free thermal effects measurement. Based on the coupled-resonator-induced transparency (CRIT) effect, the design and principle of the biosensor is introduced in detail, and the performance of the sensor is deduced by simulations. Compared to the biosensor based on a single ring configuration, the designed biosensor has a tenfold increased Q value according to the simulation results, thus the sensor is expected to achieve a particularly high resolution. And the output signal of the sensor can eliminate the thermal influence by adopting a novel algorithm. This work is expect to have great application potentials in the areas of high-resolution refractive index measurement, such as biomedical discoveries, virus screening and drinking water safety.

Keywords: biosensor; CRIT; high resolution; free thermal effects; SOI

1. Introduction

Biosensors have attracted a growing attention in recent years. Due to high refractive index (RI) contrast that enables an exceptionally small size of resonators, biosensors based on SOI (Silicon-On-Insulator) tend to be increasingly miniaturized and integrated. Furthermore, the biosensors using the similar principle for RI sensors offer significant advantages such as label-free detection, high resolution, and superior sensitivity over other traditional sensors. Taking advantage of biosensors, multiple biological analytes (molecular, cellular, virus, proteins, DNA molecules, and biological membranes [1]) can be detected, which has many potential areas of application such as biomedical sciences [1], food industry [2], environmental monitoring [3], national defense industry [4], and pharmaceutical industry [5].

The principle of such sensors is based on the interaction of the evanescent field outside the propagating waveguide with analytes in the cladding. Ambient RI changes (resulting from the changes of solution concentration or the variation in the number of binding events on the surface of the waveguide) lead to the variation of the effective index of the resonator waveguide mode, thus causing a shift of the resonance wavelength [1]. By measuring the shift of resonance wavelength, the analytes of interest can be detected.

As an important parameter to evaluate the performance of microring-resonator, many studies have been conducted to obtain a high *Q* via multi-microring structures, such as series-coupled dual-microring configuration [6, 7], parallel-coupled dual-microring configuration [8, 9], and one inside ring coupled another configuration [10]. Among these configurations, an interesting effect of coupled-resonator-induced transparency (CRIT) has arisen [11]. The CRIT effect is analogous to the electromagnetically induced transparency (EIT) effect [12, 13], which is demonstrated by using both the series-coupled and parallel-coupled dual-microring configurations. According to a study by Mario *et al.* [14], who presented a comprehensive theoretical analysis of the series-coupled dual-microring system, the CRIT effect can be obtained under certain conditions, and the CRIT peak shows an extremely high *Q* factor. Analogously, taking advantage of CRIT effect, Xu *et al.* experimentally demonstrated a *Q* factor of 3.5×10^4 by using a parallel-coupled dual-microring system [8]. Numerous parallel-coupled dual-microring chips have been designed; however, none of these studies have been utilized in the field of biosensing. On the other hand, a

higher *Q* of a resonator is usually preferable since it causes a sharper resonance peak and enables easier retrieval of the exact wavelength positions of peaks or valleys. As a result, a higher *Q* value of resonator contributes to a higher resolution of the sensor. Therefore, the CRIT effect offers a potential and interesting way to enhancing the *Q* value of microring systems and further the resolution of biosensors [15].

In an ideal case, biosensors should avoid the influence of environmental factors such as temperature variations. Unfortunately, due to the positive thermo-optic coefficient of silicon of $\kappa_{Si} \approx 1.8 \times 10^{-4}$ RIU/K [16], the detection limit of sensors is often restricted to the level of 10^{-6} refractive index units (RIU) or worse. Therefore, the influence of temperature on the RI measurement cannot be ignored.

There are mainly three methods for thermal noise reduction: temperature controlled by devices, athermal-waveguide-based configurations, and on-chip temperature drift compensation via referencing resonator [17]. One of the effective methods employs an active control of temperature via additional devices, such as a thermo-electric cooler or a Peltier heat pump, which stabilizes the temperature to a small range. However, it comes with the drawbacks such as bulky size, high cost and integrating difficulties. Another method utilizes the different polarities of thermo-optic coefficients of liquid analytes (e.g., water has a negative thermo-optic coefficient of $\kappa_{H_2O} = -10^{-4}$RIU/K [14]) and the waveguide materials [18, 19, 20, 21]. By adjusting the cross-section of waveguide, the fraction of light in both materials can be controlled to eliminate the dependence of the waveguide effective index on temperature. This method intrinsically achieves temperature compensation, but limits the type of buffer liquid of the biological analyte (to only water) and imposes strict requirements of device design and fabrication. In the third method, numerous researchers demonstrated that temperature drift can be compensated by introducing an on-chip referencing resonator [16, 18, 22]. This can be achieved via two parallel microring resonators on the same chip. The differential result of both resonators is the corrected sensing signal. This design is solvent independent; however, it is hard to meet the requirement that the microring resonators are identical and in good thermal contact with each other. Furthermore, the thermal constants of the sensor ship limit the temperature compensation in frequency.

This study proposes and investigates a biosensor design based on the parallel-coupled dual-microring resonator configuration in SOI with free thermal effects. The sensing performance of the dual-microring based biosensor is also compared with the single-microring based biosensor. Compared to other on-chip temperature compensation approaches, this design can obtain an extraordinarily high resolution and compensates the influence of temperature without the need for any exterior structure/components. Furthermore, a novel algorithm for sensing is presented based on the designed structure.

2. Theoretical analysis and device design

The schematic of the typical single ring configuration is shown in Fig.1 (a). Our proposed biosensor (see the schematic diagram in Fig.1 (b)) is a parallel-coupled dual-microring configuration, which is composed of two micro-ring resonators coupled by two bus waveguides in parallel. The ring 2 is designed as the sensing element to contact the analyte, and the other parts of the device is covered by a cladding layer (PDMS or SU8). However, the region on top of the ring 2 is opened to form a reservoir to contain the liquid sample. The 3D visualization of the proposed sensor is shown in Fig.1 (c).

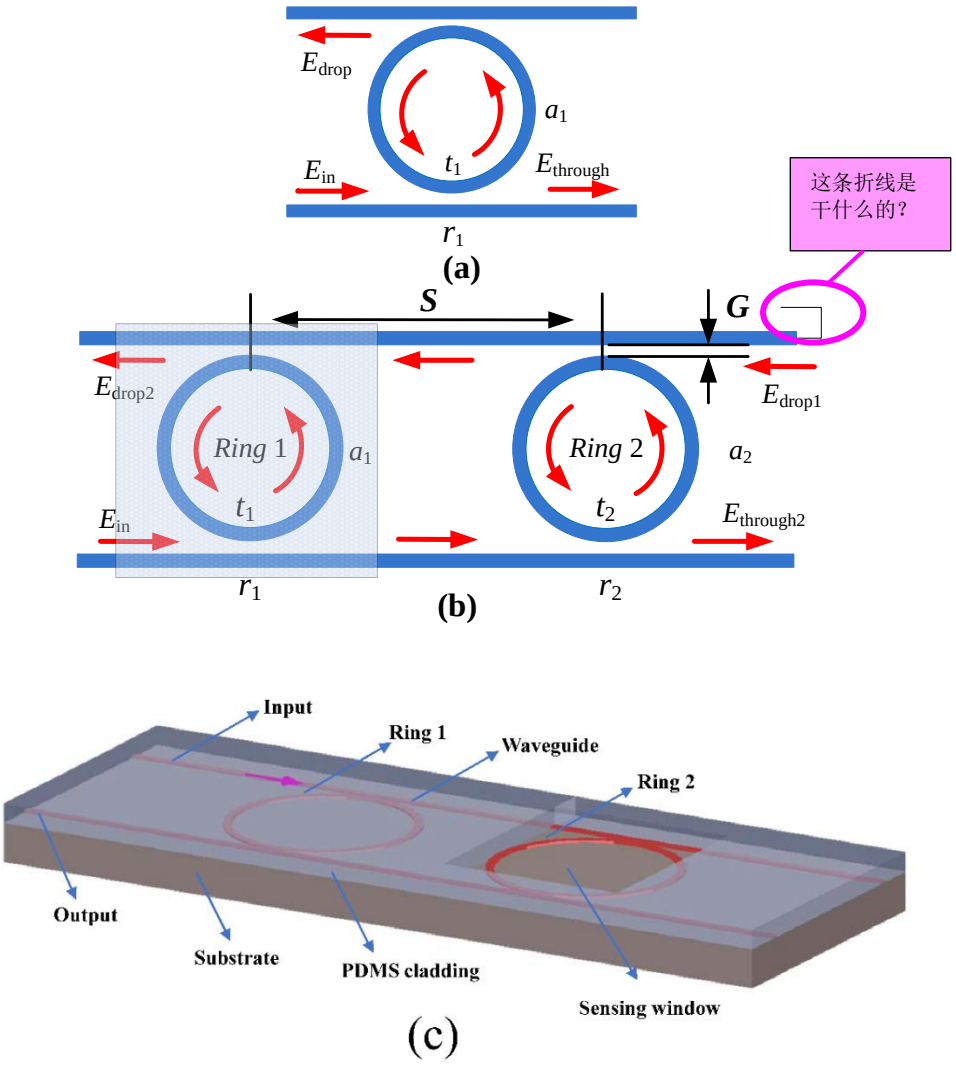

Fig. 1. Schematic diagrams of the biosensors. (a) the single ring resonator, (b) the proposed sensor using a parallel-coupled dual-microring resonator and (c) the 3D visualization of the proposed sensor.

Similar to the simplifications used by Mario et al. [14], the contributions of some geometry parameters (e.g., waveguide widths, ring gaps, and microring radii) and the transmission and reflection of the system can be simplified and deduced as two parameters: couple coefficient a_i and absorption coefficient r_i [24, 25]. The transfer matrix method (TMM) is applied to the simulation model of the designed biosensor to analyze the propagation process. The parameters involved in the simulation are shown in Table 1. These coefficients imply small waveguide losses and weak coupling between bus waveguides and rings. Furthermore, according to another study by Mario [26], all these coefficients have been demonstrated to be experimentally feasible.

Table.1 Parameters in dual-microring configuration

Parameters	Value
Radii of ring 1(R_1)	5.000 μm
Radii of ring 2(R_2)	5.003 μm
RI of ring1 (n_1)	Ranges from 3.475 to 3.4775 RIU
RI of ring2 (n_2)	3.475 RIU
Center-to-center distance (S)	15.712 μm
Reflection coupling coefficient (a_1, a_2)	0.90
Absorption coefficient (r_1, r_2)	0.99

In the single ring resonator (see Fig. 1(a)), light travels in the optical waveguide as revealed by the red arrows. The reflectance spectrum from the drop port can be analyzed using the TMM and the coupled-mode theory [14, 23], and the normalized reflectivity (R) can be obtained as Eq. (1).

In the proposed biosensor based on the parallel-coupled dual-microring configuration, the incident light (see the red arrows in Fig. 1(b)) and the reflected light of the whole system are collected from the drop-side of ring 1 (E_{drop2}). Similarly, the TMM is used to calculate the overall output spectrum at the drop port. In the TMM, the whole system is divided into three parts: ring 1, ring 2, and the bus waveguide between ring 1 and ring 2. The propagation relationship for each part can be described as the transfer matrix T_1, T_2, and L. Thus the reflectance spectrum of the dual-microring model can be derived as Eqs. (2) – (7).

$$R = \left|\frac{E_{\mathrm{drop}}}{E_{\mathrm{in}}}\right| = |d_1|^2 = \left|-\frac{(1-r_1^2)-\sqrt{a_1}\exp\left(-i\delta_1/2\right)}{1-a_1 r_1^2\exp(-i\delta_1)}\right|^2 \tag{1}$$

$$T_1 = \begin{bmatrix} \frac{\sqrt{a_1}r_1^2 e^{j\delta_2}}{r_1\left(\sqrt{a_1}-e^{j\delta_1}\right)} & -\frac{\sqrt[4]{a_1}(1-r_1)^2 e^{j\delta_1/2}}{r_1\left(\sqrt{a_2}-e^{j\delta_2}\right)} \\ -\frac{\sqrt[4]{a_1}(1-r_1)^2 e^{j\delta_1/2}}{r_1\left(\sqrt{a_1}-e^{j\delta_1}\right)} & \frac{1-\sqrt{a_1}r_1^2 e^{j\delta_1}}{r_1\left(\sqrt{a_1}-e^{j\delta_1}\right)} \end{bmatrix} \tag{2}$$

$$T_2 = \begin{bmatrix} \frac{\sqrt{a_2}r_2^2 e^{j\delta_2}}{r_2\left(\sqrt{a_2}-e^{j\delta_2}\right)} & -\frac{\sqrt[4]{a_2}(1-r_2)^2 e^{j\delta_2/2}}{r_1\left(\sqrt{a_2}-e^{j\delta_2}\right)} \\ -\frac{\sqrt[4]{a_2}(1-r_2)^2 e^{j\delta_2/2}}{r_2\left(\sqrt{a_2}-e^{j\delta_2}\right)} & \frac{1-\sqrt{a_2}r_2^2 e^{j\delta_2}}{r_2\left(\sqrt{a_2}-e^{j\delta_2}\right)} \end{bmatrix} \tag{3}$$

$$L = \begin{bmatrix} \sqrt{a_1}e^{-js/2} & 0 \\ 0 & \frac{e^{js/2}}{\sqrt{a_1}} \end{bmatrix} \tag{4}$$

where d_1 represents the transmittance from the drop port, a_i is the round-trip amplitude loss of ring i (here i = 1, 2). r_{i} is the reflection coupling coefficient between the bus waveguide and ring i. $\delta_i = \frac{2\pi n L_{\mathrm{i}}}{\lambda}$ (i = 1, 2) is the round-trip phase of ring i, in which n is the effective index of waveguides, L_i is the circumference of the microring, and λ is the wavelength. In the analysis of this parallel-coupled dual-microring configuration, the radii of both rings are nearly identical (5.000 μm vs 5.003 μm); therefore, the absorption coefficients and the coupling coefficients of the microrings are also assumed to be identical.

As shown in Fig. 1 (b), the normalized output intensified at drop port and through port, both set as E_{through2} and E_{drop1}. Thus, the relationship between the input and the output can be calculated as:

$$\begin{bmatrix} E_{\mathrm{through2}} \\ E_{\mathrm{drop1}} \end{bmatrix} = T_2 L T_1 \begin{bmatrix} E_{\mathrm{in}} \\ E_{\mathrm{drop2}} \end{bmatrix} = M \begin{bmatrix} E_{\mathrm{in}} \\ E_{\mathrm{drop2}} \end{bmatrix} \tag{5}$$

$$M = \begin{bmatrix} M_{11} & M_{21} \\ M_{12} & M_{22} \end{bmatrix} \tag{6}$$

$$D = \left|\frac{E_{\mathrm{drop2}}}{E_{\mathrm{in}}}\right|^2 = \left|\frac{M_{21}}{M_{22}}\right|^2 \tag{7}$$

where M is the overall transmission matrix of the whole system. D represents the drop port transmittance.

When both of these two microrings are under-coupled ($a < r$), the slight detuning between the resonance modes of ring 1 and ring 2 leads to a sharp dip in the middle of the peaks in the reflectance spectrum based on the CRIT effect. One typical CRIT curve obtained by the theoretical calculation is shown in Fig. 2, which constitutes a left shoulder peak, a sharp valley (i.e., the CRIT peak) and a right shoulder peak. Furthermore, these CRIT curves are periodically distributed with a free spectral range (FSR) of 21.4 nm. The sharp dip in the center of the resonance peak indicates an extremely high Q value, which is consistent with the spectra achieved by Xu et al. [9]. As the radius gap of two rings is very small, the output spectrum contains the overlap between these two rings, which means part of the light is coupled into ring 1 and ring 2 at the same time. When the light propagates through the system, the resonator reflects the light from the waveguide to the ring as a mirror. So the dual-microring configuration is actually like a multiple Fabry Pérot (FP) cavity system.

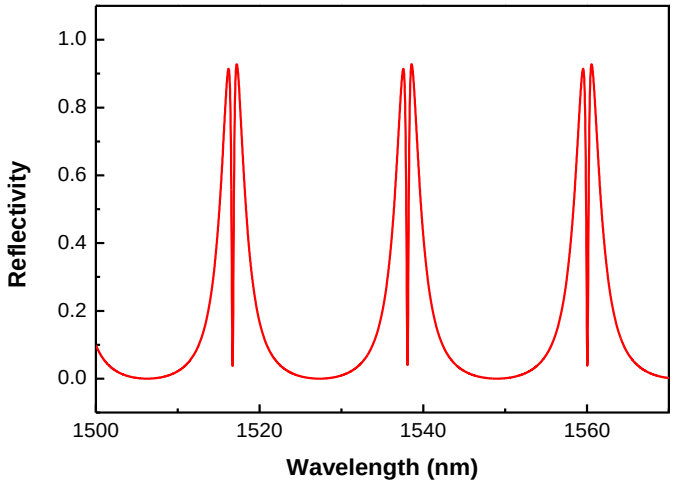

Fig. 2. CRIT spectral line of the parallel-coupled dual-microring resonator configuration. Parameters used are $a_1 = a_2 = 0.99$, $r_1 = r_2 = 0.90$.

3. Simulation results and discussion

The output spectra of the single ring configuration and the dual-microring configuration are compared in Fig. 3. It is apparent that the peak of the dual-microring configuration is much sharper that the valley of the single ring configuration with the identical coupling condition (Q value 1.2×10^4 versus 10^3). It is worth noting that both of these two values obtained via mathematical calculation are not very high as compared to some experimental results. However, the aim of our study is to compare the performances of single-ring configuration and dual-microring configuration under identical general processing conditions, not to obtain maximal values for both configurations. Sometimes, the rather large spectral width makes it difficult to find the exact position of a broad peak (or dip), especially in the presence of environmental noise. Thus, the dual-microring configuration with higher Q value yields a much smaller resolution than the single ring chip.

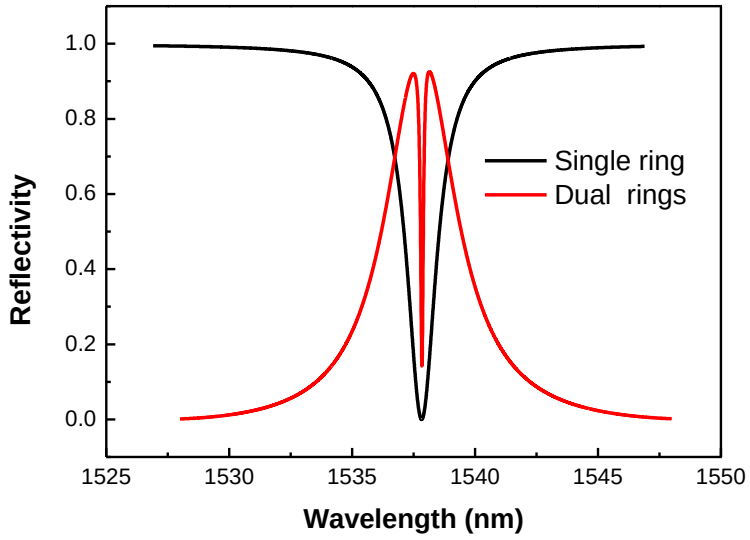

Fig. 3. Transmission/reflection of both the single ring configuration and the dual-microring configuration.

In consideration of the application of the RI sensor, the sensor will inevitably experience the effect of temperature, which will change the effective refractive indices of waveguides and will ultimately lead to a shift of resonance wavelength [23]. Based on Li [27], the dependence of the RI of Si on temperature is $\boldsymbol{n = 2 \times 10^{-4}K + 3.417}$. To mimic the thermal effect of light propagation in the silicon waveguide, in this paper, the corresponding temperature is ranged from 289 to 304 K [22]. Furthermore, the influence of temperature is imitated by a change of the refractive indices of waveguides (the RI of the waveguides ranges from 3.4750 to 3.4775). According to the outlined assumptions, Fig. 4 illustrates the reflectance spectrum with the change of temperature. According to Fig. 4, when the ambient temperature goes up, the RI of waveguides of the system (including ring 1, ring 2, and bus waveguide) increases, thus leads to the red shift of the reflectance spectrum from the drop port. However, when the right shoulder peaks of the CRIT curves in in Fig. 4 are overlapped, it can be observed that the curves are totally the same, as shown in Fig. 5 (in order to distinguish the overlapped curve, they are shifted by a short distance upward along the Y axis), and the detuning between both rings remains the same [28]. Therefore, the whole reflectance spectrum presents a red shift, and the amount of the movement is almost identical. In conclusion, the thermal effects will result in the translational red shift of the whole reflectance spectra. When the temperature is increased by approximately 3 K (the RI of system waveguide increases by approximately 0.001), the resonant wavelength will be red shifted by 0.4 nm. Simultaneously, the *Q* value remains stable because the shape of CRIT curve remains unchanged.

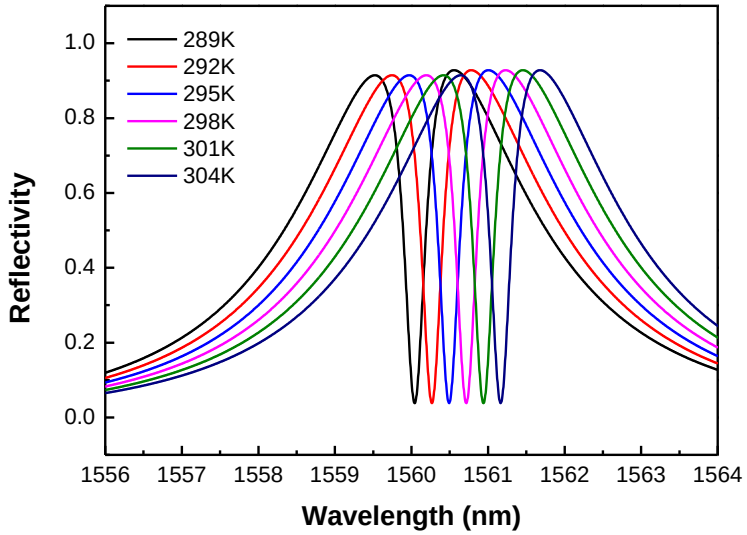

Fig. 4 Reflectance spectra of the dual-microring configuration at different temperatures. Here both n_1 and n_2 are changed.

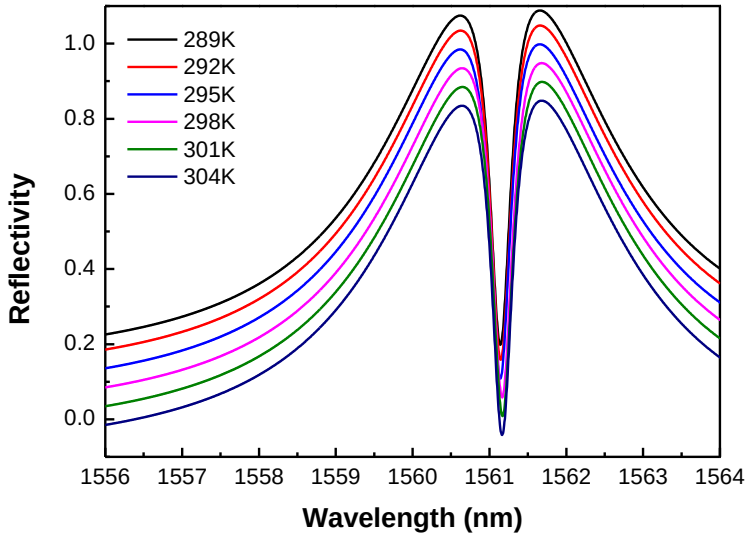

Fig. 5. Reflectance spectra of the dual-microring configuration the right shoulder peaks in Fig. 4 are artificially overlapped. Here both n_1 and n_2 are changed.

In the design of the proposed biosensor (see Fig. 1(c)), the open window allows ring 2 to contact and measure the changes of the analyte, while ring 1 is covered by a cladding material to avoid the contact with the analyte. This process is simulated by changing the RI of ring 2 and fixing that of ring 1. The obtained reflectance spectra are illustrated in Fig. 6. When the waveguide RI of ring 2 (n_2) increases (from 3.475 to 3.4775) while the waveguide RI of ring 1 remains the same (3.475), the reflectance curve presents a red shift and the Q value goes lower. Nevertheless, the Q value ($\mathbf{2 \times 10^3}$) is still higher than that of the single ring configuration ($\mathbf{1 \times 10^3}$).

However, when the right shoulder peaks of the CRIT curves are artificially overlapped for comparison as shown in Fig. 7, it is interesting to see that the CRIT resonance dips have slight blue shifts with the increase of the RI of ring 2. Thus, when the RI of ring 2 is increased, there is not only a red shift of the

whole reflectance spectrum, but also a superposed blue shift of the CRIT resonance dips. The reason of this phenomenon can be explained as follows. When the light is coupled in the single ring resonator, it will experience several coupling progresses. The system of two dual-microring configuration is equivalent to a series of FP cavity combination. The output signal of the system is formed by the light though a multi-FP-like cavity system. As n_2 increases, the output of ring 2 will produce a red shift, thus the right shoulder peak experiences a red shift. However, in case of the CRIT peak originating from the overall system output, such change leads to the variation of one FP cavity in the system, which is different from the output of the single ring configuration. Thus the red shift of CRIT peak is less than that of right shoulder peak since other parts of system alleviate the variation. And a blue shift can be observed when all curves are marked at the right shoulder peak. The change of temperature only causes a translational red shift. By measuring the blue shift, the changes of analyte can be characterized, regardless of the temperature change.

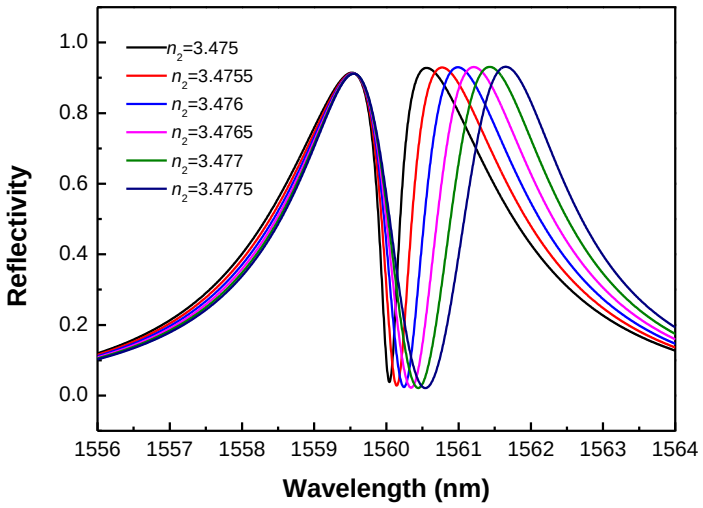

Fig. 6. Reflectance spectra of the dual-microring configuration with a change of the resonator waveguide refractive index n_2 of ring 2. Here n_1 of ring 1 remains constant.

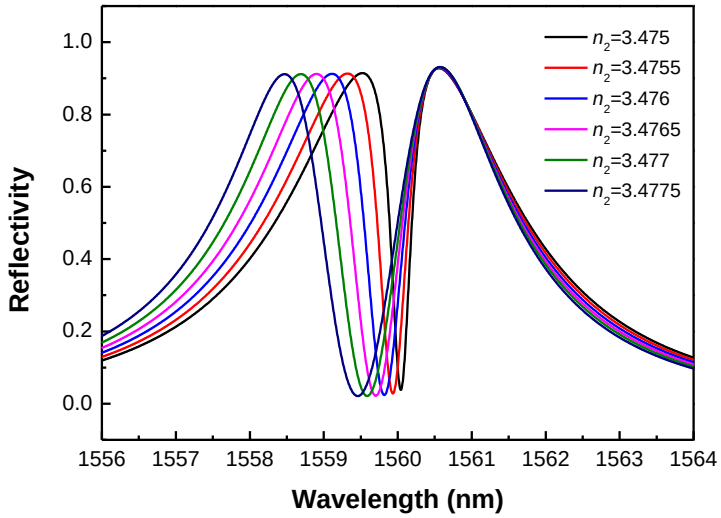

Fig. 7. Reflectance spectra of the dual-microring configuration after the right shoulder peaks in Fig. 6 are artificially overlapped. Here only n_2 of ring 2 is changed while n_1 of ring 1 remains constant.

Fig. 8 summarizes the resonance wavelength shifts of the dual-microring configuration with the change of RI. The change of resonant wavelength with respect to different temperatures (RI of all the waveguides in the system) is also shown in Fig. 8. The CRIT peaks present a red shift due to the variation of temperature. After the overlapping of the right shoulder peak of the CRIT curve, the positions of the CRIT peaks maintain stable for different temperatures. However, the CRIT peak produces a blue shift only when the analyte is attached to ring 2. Since the CRIT peak shifts in the opposite direction, the changes of analyte can be characterized easily.

The sensitivity (S) of biosensors is defined as the ratio of the resonance wavelength shift ($\boldsymbol{\Delta\lambda}$) to the changes in ambient RI ($\boldsymbol{\Delta n_c}$). According to Fig. 8, the sensitivities of the dual-microring and the single ring configuration are 200 nm/RIU and 400 nm/RIU, respectively. Although the sensitivity of the dual-microring is lower than that of single ring configuration, the highly increased Q value of the characteristic peak can greatly reduce the fitting error during data processing, which is the main source of the ultrahigh RI measurement. With a high-resolution optical spectrum analyzer (0.01 picometer), the sensitivity of the sensor can reach $\boldsymbol{5 \times 10^{-8}}$ RIU. Furthermore, the consequence of the thermal effect can be easily removed during the analyte detection by the use of this method, and the dual-microring structure resolution is much higher than the single ring resolution.

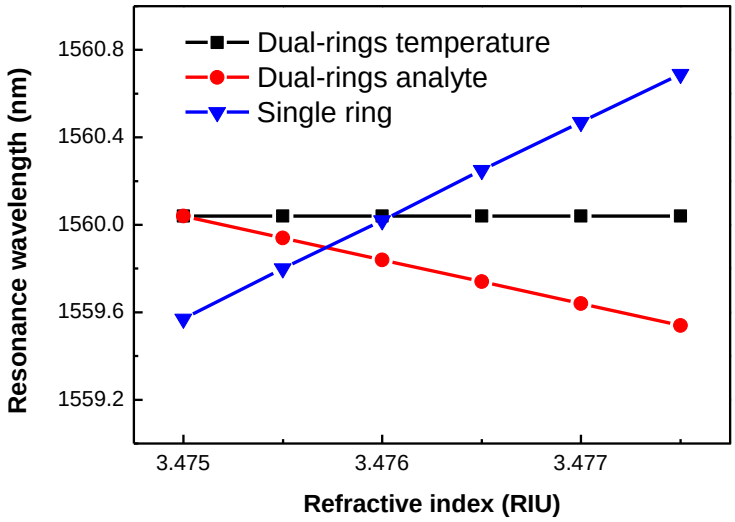

Fig. 8. The CRIT peak of the dual-microring configuration with respect to different RIs/temperatures; resonance wavelengths of single ring configuration due to different RIs.

4. Conclusion

In this paper, the parallel-coupled dual-microring based biosensor in SOI is proposed and analyzed by the TMM. The simulation results show that the ambient temperature variation causes a red shift of the overall reflectance spectra. However, the RI results of the analytes cause a blue shift blue of the CRIT resonance dip, when the right shoulder peaks of the CRIT curves are aligned artificially. This enables to completely free the sensor from thermal effects. The biosensor can achieve a sensitivity of 200 nm/RIU as compared to the sensitivity of the single-ring configuration 400 nm/RIU. However, the Q value of the dual-microring configuration can reach 10^4, which is approximately tenfold higher than that of the single ring configuration. With excellent performance and thermal-free characteristics, the device with the dual-microring configuration offers great potential for high-resolution biosensing applications.

Acknowledgements: This study was financially supported by the National Natural Science Foundation of China (No. 61471255, 61474079, 61501316, 51505324 and 51622507), the Basic Research Program of Shanxi for Youths (No. 2014021023-3 and 2015021092), the Shanxi Provincial Foundation for Returned Scholars (2015-047), and 863 project (2015AA042601).

Author contributions: The initial idea was proposed by Sang Shengbo. Jian Aoqun and Ji Jianlong built the dual-microring configuration model. The parameter design was completed by Zhang Qiang. Tang Haiquan and Duan Qianqian performed the system simulation and data analysis. Zhang Xuming revised the manuscript. All authors contributed to the writing of the manuscript.

Conflicts of Interest: The authors declare no conflict of interest. The founding sponsors had no role in the design of the study; in the collection, analyses, or interpretation of data, in the writing of the manuscript, and in the decision to publish the results.

References

[1] Fan, X. D.; White, I. M.; Shopova, S. I.; Zhu, H. Y.; Suter, J. D.; Sun, Y. Z. Sensitive optical biosensors for unlabeled targets: A review. *Anal. Chim. Acta.* **2008**, 620**,** 8-26.

[2] Baaske, M.; Vollmer, F. Optical resonator biosensors: molecular diagnostic and nanoparticle detection on an integrated platform. *Chem. Phys. Chem*. **2012**, 13,427-436.

[3] Claes, T.; Molera, J. G.; Vos, K. D.; Schacht, E.; Baets, R.; Bienstman, P. Label-free biosensing with a slot-waveguide-based ring resonator in silicon on insulator. *IEEE Photonics J*. **2009**, 1, 197-204.

[4] Barrios, C. A. Optical slot-waveguide based biochemical sensors. *Sens.* **2009**, 9, 4751-4765.

[5] Yuan, G.H.; Gao, L.; Chen,Y.R.; Liu, X.L.; Wang, J.; Wang, Z.R. Improvement of optical sensing performances of a double-slot-waveguide-based ring resonator sensor on silicon-on-insulator platform. *Optik*. **2014**, 125, 850-854.

[6] Kwon, M. S.; Steier, W. H. Microring-resonator-based sensor measuring both the concentration and temperature of a solution. *Opt. Express.* **2008**, 16**,** 9372-9377.

[7] Mario, L. Y.; Lim, D. C. S.; Chin, M. K. Proposal for an ultranarrow passband using two coupled rings. *IEEE Photon. Technol. Lett*. **2007**, 19**,** 1688-1690.

[8] Xu, Q. F.; Sandhu, S.; Povinelli, M. L.; Shakya, J.; Fan, S. H.; Lipson, M. Experimental realization of an on-chip all-optical analogue to electromagnetically induced transparency. *Phys. Rev. Lett*. **2006**, 96**,** 123901.

[9] Xu, Q. F.; Shakya, J.; Lipson, M. Direct measurement of tunable optical delays on chip analogue to electromagnetically induced transparency. *Opt. Express.* **2006**, 14**,** 6463-6468.

[10] Su, B. Q.; Wang, C. X.; Kan, Q.; Chen, H. D. Compact silicon-on-insulator dual-microring resonator optimized for sensing. *J. Lightwave Technol*. **2011**, 29**,** 1535-1541.

[11] Smith, D. D.; Chang, H.; Fuller, K. A.; Rosenberger, A. T.; Boyd, R. W. Coupled-resonator-induced transparency. *Phys. Rev. A*. **2004**, 69**,** 63804.

[12] Xiao, Y. F.; He, L.; Zhu, J. et al. Electromagnetically induced transparency-like effect in a single polydimethylsiloxane-coated silica microtoroid[J]. *Appl. Phys. Lett*. **2009**, 94(23): 231115.

[13] Peng, B.; Özdemir, Ş. K.; Chen, W. et al. What is and what is not electromagnetically induced transparency in whispering-gallery microcavities[J]. *Nature Commun.* **2014**, 5.

[14] Mario, L. Y.; Chin, M. K. Optical buffer with higher delay-bandwidth product in a two-ring system. *Opt. Express.* **2008**, 16, 1796-1807.

[15] Zhu, J.; Ozdemir, S. K.; Xiao, Y. F. et al. On-chip single nanoparticle detection and sizing by mode splitting in an ultrahigh-Q microresonator[J]. *Nature Photon.* **2010**, 4(1): 46-49.

[16] Fard, S.T.; Donzella, V.; Schmidt, S.A.; Flueckiger, J.; Grist, S.M.; TalebiFard, P.; Wu, Y.C.; Bojko, R.J.; Kwok, E.; Jaeger, N.A.F.; Ratner, D.M.; Chrostowski, L. Performance of ultra-thin SOI-based resonators for sensing applications. *Opt. Express.* **2014**, 22, 14166-14179.

[17] Gylfason, K.B.; Carlborg, C.F.; Ka´zmierczak, A.; Dortu, F.; Sohlstrom, H.; Vivien, L.; Barrios, C.A.; Wijngaart, W.; Stemme, G. On-chip temperature compensation in an integrated slot-waveguide ring resonator refractive index sensor array. *Opt. Express.* **2010**, 18, 3226-3237.

[18] Xu, D.X.; Vachon, M.; Densmore, A.; Ma, R.; Janz, S.; Delâge, A.; Lapointe, J.; Cheben, P.; Schmid, J.H.; Post, E.; Messaoudène, S.; Fédéli, J.M. Real-time cancellation of temperature induced resonance shifts in SOI wire waveguide ring resonator label-free biosensor arrays. *Opt. Express.* **2010**, 18, 22867-22879.

[19] Chu, S.; Little, B.; Pan, W.; Kaneko, T.; Sato, S.; Kokubun, Y. An eight-channel add-drop filter using vertically coupled microring resonators over a cross grid. *IEEE Photon. Technol. Lett.* **1999**, 11, 691-693.

[20] Lee, J.; Kim, D.; Ahn, H.; Park, S.; Kim, G. Temperature dependence of silicon nanophotonic ring resonator with a polymeric overlayer. *J. Lightwave Technol*. **2007**, 25, 2236-2243.

[21] Ye, W.; Michel, J.; L. Kimerling Athermal high-index-contrast waveguide design. *IEEE Photon. Technol. Lett*. **2008**, 20, 885-887.
[22] Abdulla, S.M.C.; Boer, B.M.; Pozo, J.M.; Berg, J.H.; Abutan, A.; Hagen, R.A.J.; Cascio, L.; Harmsma, P. J. Sensing platform based on micro-ring resonator and on-chip reference sensors in SOI. *Proc. of SPIE.* **2014**, 8990, 89900W.
[23] Robinson, J. T.; Chen, L.; Lipson, M. On-chip gas detection in silicon optical microcavities. *Opt. Express.* **2008**, 16**,** 4296-4231.
[24] Lu, Y.; Huang, X. H.; Fu, X. Y.; Wen, W. Q.; Yao, J. Q. Interference effect in a dual microresonator-coupled Mach-Zehnder interferometer. *Opt. Appl*. **2012**, 42**,** 23-29.
[25] On-chip temperature compensation in an integrated slot-waveguide ring resonator refractive index sensor array. *Opt. Express*. **2010**, 18, 3226-3237.
[26] Mario, L. Y. Micro-ring devices and circuits. PhD. Thesis of Nanyang Technological University 2009.
[27] Li H.H. Refractive index of silicon and germanium and its wavelength and temperature derivatives. *AIP Publishing.* **1980**, 9, 561-658.
[28] Rosenblum, S.; Lovsky, Y.; Arazi, L. et al. Cavity ring-up spectroscopy for ultrafast sensing with optical microresonators [J]. *Nature Commun.* **2015**, 6.